Minimizing Stopping Distance on Split Friction via Steering and Individual Wheel Braking Optimization

Ektor Karyotakis[1,2], Mats Jonasson[3], Derong Yang[1], and Jonas Sjöberg[2]

[1] Vehicle Energy and Motion Control, Volvo Car Corporation, SE-405 31 Gothenburg, Sweden
ektor.karyotakis@volvocars.com,
[2] Department of Electrical Engineering, Chalmers University of Technology, SE-412 96 Gothenburg, Sweden
[3] Department of Maritime and Mechanical Engineering, Chalmers University of Technology, SE-412 96 Gothenburg, Sweden

Abstract. Braking hard on a split friction road generates asymmetric brake forces, creating a yaw moment disturbance. For most drivers, it is challenging to counteract the disturbance using steering, which could make the vehicle deviate from the lane and potentially into a dangerous situation. A straightforward way to keep a vehicle in its lane is to apply equal brake force to all wheels based on the lowest level of road friction. Unfortunately, this method has the downside of significantly reducing the vehicle's braking capacity, resulting in an increased stopping distance. Hence, the braking capabilities can be noticeably improved by incorporating automated steering compensation. This paper suggests a solution for optimizing steering jointly with individual wheel braking. The proposed approach determines the upper deceleration limit while ensuring the vehicle stays on its intended path. The upper deceleration limit depends on the friction asymmetry between the vehicle's low and high friction sides. In cases of small friction asymmetry, steering is an effective means of maximizing braking at each wheel. However, at large friction asymmetry, steering compensation saturates, rendering it impossible to attain maximum braking at each wheel. Also, the vehicle must drift to maintain a straight path during braking.

Keywords: vehicle, braking, split, friction, optimization, asymmetry

1 Introduction

At least one-tenth of fatal crashes in the US involve skidding pre-impact [1]. Skidding happens when one or more tires exceed their friction limits and lose grip, affecting the vehicle's stability. This phenomenon typically appears when braking hard on a slippery road. Split friction is a special case of a slippery road when one side of the vehicle lies on a low friction patch, such as snow or oil spillage, while the other is on the pavement. The Anti-lock Braking System

(ABS) reduces the brake forces on the low-friction side to prevent wheel lock, but this creates an asymmetry that generates a yaw moment disturbance [2]. Most ABSs expect the driver to counter the disturbance by steering. Nonetheless, only skilled drivers can stabilize the vehicle as the yaw moment disturbance can be abrupt and unexpected [3]. Especially when an autonomous function initiates braking, distracted drivers take extra time to reject the disturbance and stabilize the vehicle [4]. In either case, automating yaw moment disturbance rejection should improve braking performance.

Braking hard on split friction can be summed into three cases, illustrated in Fig. 1. First, case A without any steering compensation is shown. The vehicle departs from the lane, and the stopping distance might be the shortest possible, provided the vehicle remains stable. The most straightforward approach to remaining in-lane is to make the brake forces equal to the low-friction side, which increases the stopping distance (B in Fig. 1). Case C is the best-case scenario where the stopping distance is the shortest while the vehicle stays in its lane.

Contributions in literature have primarily focused on designing a controller for steering, assuming the ABS handles the brake control, as in [2, 3, 5]. In [2], a sliding mode controller performs steering compensation control, focusing on robustness to parameter uncertainty. In [3, 5], the predictive path is considered, adapting the steering controller based on receding horizon LQR control. The brakes and steering system can be electronically controlled and coordinated in an autonomous vehicle for improved performance, as in [6].

There is a limit to the deceleration that can be achieved without deviating from the lane leading to the shortest stopping distance (C in Fig. 1) and is dependent on the friction coefficient of each vehicle side. There are two complications to reaching the shortest distance. First, the brake forces at each wheel and steering must be optimized simultaneously to reach the shortest distance. Optimizing braking through the ABS first and then the steering leads to a suboptimal stopping distance (between points B and C). Secondly, uncertainty in friction estimation and simplifications in the tire limits also affect optimality. An alternative to perfect knowledge of friction is to react proactively. Machine learning algorithms in perception sensors have been used to predict the road state ahead of the vehicle with adequate accuracy [7]. This knowledge can be used to improve control on roads with varying friction.

This paper proposes a method for finding the upper limit of deceleration for straight-line braking while staying in-lane by optimally controlling individual brake forces and steering. The underlying assumption is that the friction coefficient and the tire's force-slip characteristics are instantaneously known before or when the ABS activates. The upper deceleration limit is sought from a nonlinear optimization problem based on a two-track vehicle dynamics model with load transfer and a combined slip tire model with friction circle limitations. The following constraints are added to ensure the vehicle maintains a straight path during braking: 1) zero yaw rate, 2) zero yaw moment balance, and 3) zero acceleration perpendicular to the path. Finally, friction's effect on the upper deceleration limit is investigated using the friction asymmetry measure, defined as the difference in friction between each vehicle side.

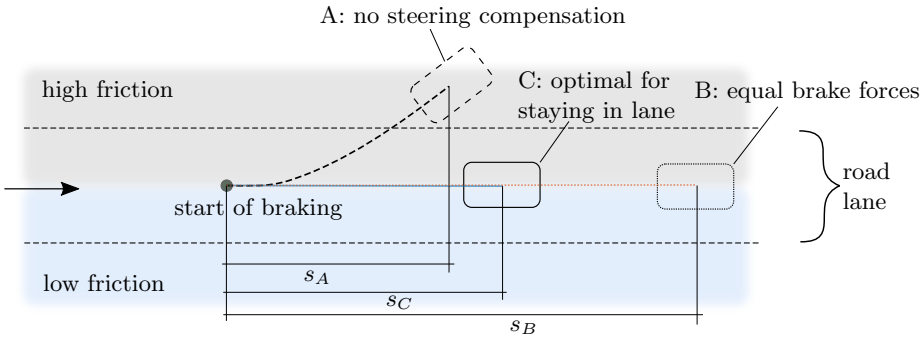

Fig. 1: Paths of 3 vehicles (A, B, C) braking on split friction with different brake/steering control. The stopping distance (s_A, s_B, s_C) is indicated for each.

2 Nonlinear two-track vehicle model

The objective of the vehicle model is to describe the dynamics of a vehicle braking hard on a straight-line without rotating. For this purpose, a two-track vehicle model is introduced with nonlinear tires. Each tire's friction limitations are modelled along with load transfer and combined slip, which influence the available capacity of the wheels during combined braking and steering.

2.1 Friction circle

The tire forces are typically modelled to be limited within a friction ellipse. Assuming that the road friction coefficient is isotropic, i.e., the same longitudinally and laterally ($\mu_{xij} = \mu_{yij} = \mu_{ij}$), the friction ellipse is simplified into a circle

$$\sqrt{F_{xij}^2 + F_{yij}^2} \leq F_{\max,ij} \tag{1}$$

where F_{xij} is the longitudinal tire force, F_{yij} the lateral tire force, and $F_{\max,ij}$ each tire's force limit defined as $F_{max,ij} = \mu_{ij} F_{zij}$. Also, i refers to the front $(i = 1)$ or rear $(i = 2)$ axle, and j to the left $(j = 1)$ or rear $(j = 2)$ side.

The utilized force is derived from (1) as

$$f_{uij} = \frac{\sqrt{F_{xij}^2 + F_{yij}^2}}{F_{\max,ij}} \leq 1 \tag{2}$$

and shows how much of the force limit is utilized at each tire.

2.2 Equations of motion

A two-track vehicle model with front-wheel steering is shown in Fig. 2(a). The same steering angle δ is assumed for the left and right wheels. As will be presented

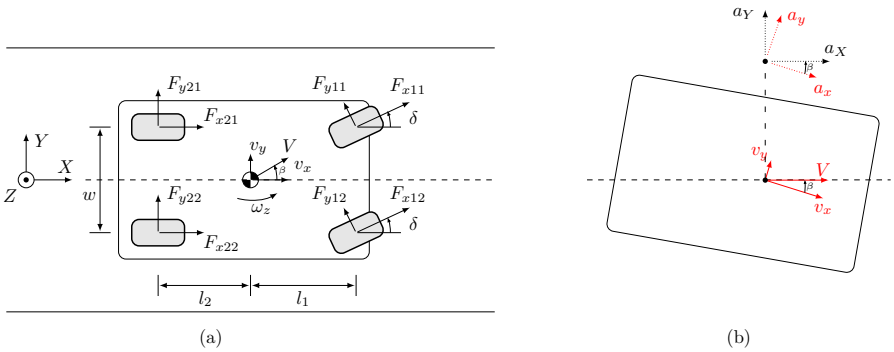

Fig. 2: (a) Two-track vehicle model; (b) Special case of body rotation with the total velocity vector V parallel to the intended path and corresponding acceleration vector transformation

in the results, countering the yaw moment disturbance requires that the body is tilted by a side slip angle β, which is defined as

$$\beta = \arctan\left(\frac{v_y}{v_x}\right) \tag{3}$$

In this way, the velocity vector V is oriented along the path, see Fig. 2(b). Due to β, a coordinate transformation of the acceleration vectors along V is needed. Specifically, the acceleration vectors in the body-fixed system xyz are transformed into the global system XYZ as

$$\begin{pmatrix} a_X \\ a_Y \end{pmatrix} = \begin{pmatrix} \cos\beta & \sin\beta \\ -\sin\beta & \cos\beta \end{pmatrix} \begin{pmatrix} a_x \\ a_y \end{pmatrix} \tag{4}$$

The acceleration along the path a_X is the optimization goal, while the acceleration perpendicular to the path a_Y is constrained to zero to ensure that the vehicle does not move laterally. The motion of a vehicle needs then be described. The equations of planar motion are given as follows

$$F_x = m\,a_x = m(\dot{v}_x - \omega_z v_y) \tag{5}$$
$$F_y = m\,a_y = m(\dot{v}_y + \omega_z v_x) \tag{6}$$
$$M_z = I_z \dot{\omega}_z \tag{7}$$

where the total forces and moments in the body-fixed system xyz are given by

$$F_x = (F_{x11} + F_{x12})\cos\delta - (F_{y11} + F_{y12})\sin\delta + F_{x21} + F_{x22} \tag{8}$$
$$F_y = (F_{x11} + F_{x12})\sin\delta + (F_{y11} + F_{y12})\cos\delta + F_{y21} + F_{y22} \tag{9}$$
$$\begin{aligned} M_z = {} & ((F_{x11} + F_{x12})\sin\delta + (F_{y11} + F_{y12})\cos\delta)\,l_1 \\ & - (F_{y21} + F_{y22})\,l_2 \\ & + ((-F_{x11} + F_{x12})\cos\delta + (F_{y11} - F_{y12})\sin\delta - F_{x21} + F_{x22})\,\frac{w}{2} \end{aligned} \tag{10}$$

Note that motion resistances, such as the air drag and rolling resistance, are ignored. Further, steady-state load transfer is included in the model changing the force limit in (1), i.e., $F_{\max,ij}(F_{xij}, F_{yij}, \delta)$, as in [8].

2.3 Tire model with combined slip

When braking and cornering are pushed to the limits, the tire characteristics like stiffness change nonlinearly with slip and vertical load. This phenomenon is typically modelled through the combined slip [9], and is expressed as

$$\sigma_{ij} = \sqrt{\sigma_{xij}^2 + \sigma_{yij}^2} \tag{11}$$

where σ_{xij} is the longitudinal and σ_{yij} the lateral slip of each tire, defined as

$$\sigma_{yij} = \frac{\tan \alpha_{ij}}{1 + \sigma_{xij}} \approx \frac{\alpha_{ij}}{1 + \sigma_{xij}} \tag{12}$$

A small-angle approximation is made for the tire lateral slip angles α_{ij}, while the σ_{xij} are unknown in the optimization and do not need to be defined. The lateral slip angles α_{ij} are obtained by transforming the velocity vectors from the wheels to the body-fixed system xyz [8], giving

$$\alpha_{ij} \approx \left[\delta - \tfrac{v_y + l_1\omega_z}{v_x - \frac{w}{2}\omega_z}, \delta - \tfrac{v_y + l_1\omega_z}{v_x + \frac{w}{2}\omega_z}, -\tfrac{v_y - l_2\omega_z}{v_x - \frac{w}{2}\omega_z}, -\tfrac{v_y - l_2\omega_z}{v_x + \frac{w}{2}\omega_z}\right]^\mathsf{T} \tag{13}$$

The magnitude of the combined force of each tire is modelled with the hyperbolic tangent model (adapted from [8]) as

$$F_{ij} = F_{\max,ij} \tanh\left(\frac{C_i \sigma_{ij}}{F_{\max,ij}}\right) \tag{14}$$

where C_i is the tire stiffness. The longitudinal and lateral tire forces are then split using the combined slip and the combined force as

$$F_{xij} = \frac{\sigma_{xij}}{\sigma_{ij}} F_{ij} \tag{15}$$

$$F_{yij} = \frac{\sigma_{yij}}{\sigma_{ij}} F_{ij} \tag{16}$$

2.4 Optimization problem: maximum deceleration

The shortest stopping distance is sought when braking on a split friction surface. Another way to examine the problem is by maximizing the deceleration until the vehicle reaches a complete stop. Under the assumption that the dynamics are ignored, this would lead to the shortest stopping distance. A quasi-steady state is reached as deceleration reaches a steady state after initial transients, while speed reduces to zero. Specifically, the longitudinal acceleration in the global system a_X is the minimization variable, calculated from (4). The global lateral

acceleration a_Y along with the derivatives of the lateral states, i.e., $[\dot{v}_y, \dot{\omega}_z]$, are set to zero to avoid lateral translation of the body. The body's rotation is also unwanted; thus, the sum of moments M_z from (10) should be zero, along with a zero yaw rate constraint for straight-line braking. Setting $\omega_z = 0$, the lateral slip angles from (13) are reduced to

$$\alpha_{ij} = [\delta - \beta,\ \delta - \beta,\ \ -\beta,\ \ -\beta]^\intercal \tag{17}$$

The tire forces are calculated from (15)-(16). The combined force from the hyperbolic tangent model (14) is bounded, as are the forces (15)-(16) and already satisfy the friction circle limitations. However, adding the inequalities (1) helps the optimization algorithm approach the equilibrium point from the correct side and avoid numerical instabilities. In fact, $F_{\max,ij}$ is multiplied by a scaling factor

$$\sqrt{F_{xij}^2 + F_{yij}^2} \leq k\, F_{\max,ij} \tag{18}$$

with $k < 1$ to ensure the optimization finds a unique solution. That is because the hyperbolic tangent exhibits a plateau at the peak of the tire force – slip curve, and there are several slip values for the maximum tire force. Staying to the left of the peak is desirable. The utilized force (2) is also adjusted accordingly.

The optimization problem is expressed in compact form as

$$\begin{aligned}
\min_{\sigma_{xij}, F_{xij}, F_{yij}, \delta, \beta} \quad & a_X(F_{xij}, F_{yij}, \delta, \beta) \\
\text{s.t.} \quad & a_Y(F_{xij}, F_{yij}, \delta, \beta) = 0 \\
& \dot{\omega}_z(F_{xij}, F_{yij}, \delta) = 0 \\
& \omega_z = 0 \\
& F_{xij} - \frac{\sigma_{xij}}{\sigma_{ij}(\sigma_{xij}, \delta, \beta)} F_{ij}(\sigma_{xij}, F_{xij}, F_{yij}, \delta, \beta) = 0 \\
& F_{yij} - \frac{\alpha_{ij}(\delta, \beta)}{1 + \sigma_{xij}} \frac{1}{\sigma_{ij}(\sigma_{xij}, \delta, \beta)} F_{ij}(\sigma_{xij}, F_{xij}, F_{yij}, \delta, \beta) = 0 \\
& \sqrt{F_{xij}^2 + F_{yij}^2} - k\, F_{\max,ij}(F_{xij}, F_{yij}, \delta) \leq 0
\end{aligned} \tag{19}$$

The unknown variables $q = [\sigma_{xij}, F_{xij}, F_{yij}, \delta, \beta]^\intercal$ are 14 in total. There are 11 equality and 4 inequality constraints. The optimization problem is solved using Matlab's nonlinear programming solver *fmincon*.

3 Effects of friction asymmetry

The friction coefficient on each vehicle side is set to the same value, i.e., $\mu_{1j} = \mu_{2j} = \mu_j$. The friction asymmetry between the left and right vehicle side is defined as

$$\Delta_\mu = \mu_2 - \mu_1 \tag{20}$$

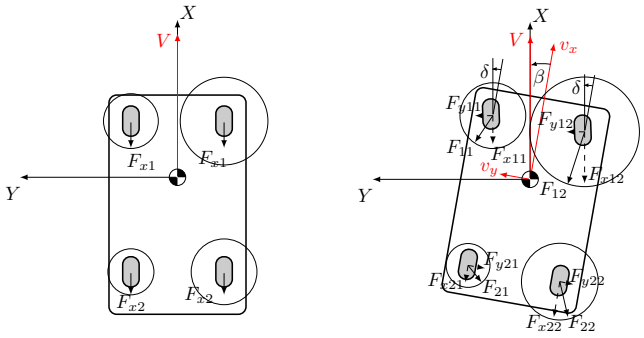

Equal Brake Force (EBF) strategy Minimization (M) strategy

Fig. 3: Sketches of a vehicle under two brake/steering control strategies and corresponding tire forces on a split friction road

The friction asymmetry measure is used to evaluate the effect of friction on the optimization's (19) outputs.

Fig. 3 presents two brake/steering control strategies. First is the equal brake force (EBF) strategy, in which the low-friction side dictates the brake forces, and there is no counter-steering required as no yaw moment disturbance is generated. Second, is the minimization (M) strategy, which comes by solving the optimization problem (19). A constant side slip angle β is depicted for the M strategy, which is observed in the optimization solutions, see Fig. 5.

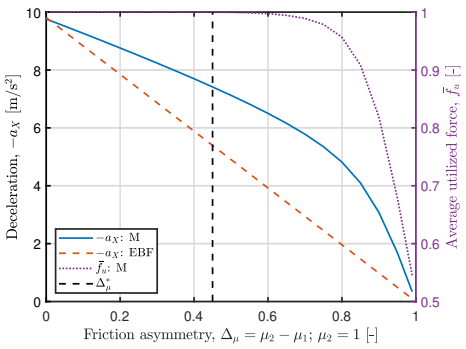

(a) Deceleration vs friction asymmetry Δ_μ for two strategies, and average utilized force of all wheels $\bar{f}_u$ for the optimal one

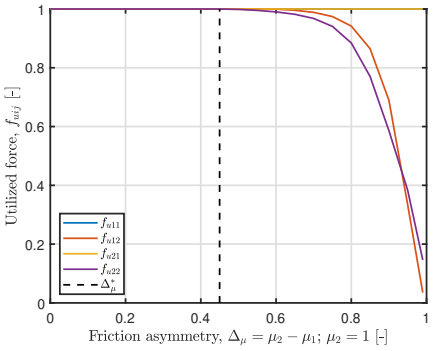

(b) Utilized force of each wheel vs friction asymmetry Δ_μ

Fig. 4: Friction asymmetry effects on deceleration and force capacity of the tires. The point of counter-steering saturation is indicated with Δ_μ^*.

The friction asymmetry Δ_μ is computed for a range of friction coefficient values for the left side of the vehicle μ_1, while the right side remains at dry asphalt, i.e., $\mu_2 = 1$. In Fig. 4(a), the EBF strategy's deceleration values and the upper deceleration limit from M are depicted for increasing values of Δ_μ. At $\Delta_\mu = 0$, both vehicle sides are on dry asphalt, increasing to $\Delta_\mu = 0.95$ corresponding to black ice on the low-friction side. The average utilized force of all wheels $\bar{f}_u = \frac{1}{4}\sum_{\{i,j\}=1}^{2} f_{uij}$ is also plotted for M. The optimization curve shows a local linear relation between deceleration and friction asymmetry, up to a specific asymmetry value, $\Delta_\mu^* = 0.45$. From this value onwards, fully utilizing the tires to brake while countering the yaw moment is no longer possible, verified by observing the drop in $\bar{f}_u$. Consequently, braking needs to be reduced to the level of feasible counter-steering.

The utilized force of each wheel is plotted against the friction asymmetry in Fig. 4(b). The asymmetry value of discontinuity Δ_μ^* becomes evident, and it is the rear high-friction (right) tire that loses first the ability to utilize its capacity fully, followed by the front high-friction tire at about $\Delta_\mu = 0.15$ after. From the equation perspective, inequality (18) becomes inactive for the rear right tire after Δ_μ^*, while all the other constraints are active. The reason that the rear loses its utilization first should be connected to the load transfer towards the front during braking.

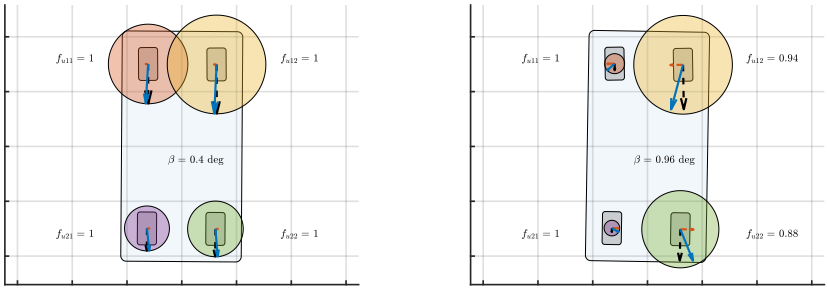

(a) $\Delta_\mu = 0.2$ (b) $\Delta_\mu = 0.8$

Fig. 5: Vehicle sketch of the optimal solution M for two friction asymmetry Δ_μ values. The friction circles are scaled based on the available load and their utilized force f_{uij} is denoted by each circle side. The body is tilted by β.

In Fig. 5, the vehicle is illustrated with its tire friction limitations for two friction asymmetry values. At small friction asymmetry (Fig. 5(a)), all tires are saturated while the vehicle orientation is close to parallel. In contrast, at large friction asymmetry (Fig. 5(b)), the forces at the high friction side are away from the limit, while the tires at the low friction side are saturated. Notably, the rear

left tire has quite a small capacity, used mainly by the required lateral forces to maintain the yaw balance and no-rotation equality constraints.

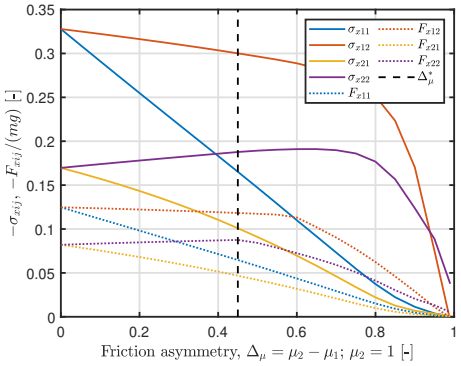

(a) Longitudinal tire slip σ_{xij} & normalized long. tire forces F_{xij} vs friction asymmetry Δ_μ

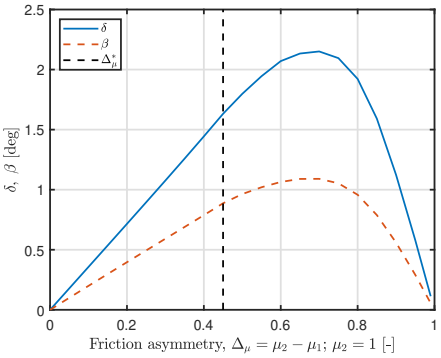

(b) Steering wheel angle δ and body side slip angle β vs friction asymmetry Δ_μ for the optimal solution

Fig. 6: Braking and steering connection to friction on a split friction road. The point of counter-steering saturation is indicated with Δ_μ^*.

Further insights are presented in Fig. 6. In Fig. 6(a), the longitudinal tire slip σ_{xij} and -forces F_{xij} are plotted against friction asymmetry. The low-friction tires (11 & 21) show an almost linear relation with Δ_μ. The rear high-friction tire displays an increasing slip σ_{x22} up to Δ_μ^*, where it reaches a peak and decreases with a different slope afterward. However, force F_{x22} keeps increasing even after Δ_μ^* up to a point, which happens as the load transfer decreases due to the decreasing braking intensity. Therefore, there is a tendency for larger capacity at the rear. In Fig. 6(b), the effect of friction on the steering angle δ and the body slip angle β is depicted. It can be seen that steering increases even after Δ_μ^*, up to approximately $\Delta_\mu = 0.7$, and decreases afterward. The slip angle β follows a similar tendency. It is important to note that a non-zero β is obtained, indicating that the vehicle drifts along the path at a slight angle, see also the sketch in Fig. 3(b) in which β is exaggerated. This drifting can be counter-intuitive to a human driver, as typically, one expects braking in a straight line with zero orientation angle. The zero β expectation also complicates geometric path-following algorithms.

4 Conclusion

This article provides the shortest stopping distance without deviating from the lane on a split friction surface. The shortest distance is obtained by simultaneously optimizing steering and individual wheel braking in a nonlinear optimization based on a two-track vehicle model with friction circle limitations.

The optimization calculates the upper limit of deceleration for staying in-lane, assuming perfect knowledge of the road friction coefficient before or when initiating braking. The upper deceleration limit is then evaluated against friction asymmetry to reveal its dependence.

The results show that significant gains in deceleration can be achieved compared to a conservative equal-brake-forces strategy. Specifically, the key conclusions from this work are the following:

- To reject the yaw moment disturbance, the vehicle requires a non-zero body side slip angle during braking.
- At large friction asymmetry, it is impossible to counter the yaw moment disturbance by steering; hence, the tires are not fully utilized.

With this knowledge, existing emergency brake functions can be improved. Correspondingly, friction asymmetry can be used in motion planning algorithms to adapt to road conditions in a better way. Future steps include establishing an optimal control algorithm and its comparison in simulations to established control algorithms that do not require any friction knowledge.

References

1. National Center for Statistics and Analysis: Traffic safety facts 2020: A compilation of motor vehicle crash data. Tech. rep., (Report No. DOT HS 813375). National Highway Traffic Safety Administration (2022). URL https://crashstats.nhtsa.dot.gov/.
2. Hebden, R.G., Edwards, C., Spurgeon, S.K.: Automotive steering control in a split-μ manoeuvre using an observer-based sliding mode controller. Vehicle System Dynamics **41**, 181–202 (2004). DOI 10.1076/vesd.41.3.181.26511
3. Yu, L., Zheng, S., Dai, Y., Abi, L., Liu, X., Cheng, S.: A feedback-feedforward steering controller designed for vehicle lane keeping in hard-braking manoeuvres on split-μ roads. Vehicle System Dynamics **60**, 1763–1787 (2022). DOI 10.1080/00423114.2020.1869274
4. Tagesson, K., Jacobson, B., Laine, L.: Driver response to automatic braking under split friction conditions. In: Proc. of the 12th International Symposium on Advanced Vehicle Control (AVEC), pp. 666–671 (2014)
5. Abi, L., Jin, D., Zheng, S., Lu, Z., Yu, L.: Dynamic coordinated control strategy of autonomous vehicles during emergency braking under split friction conditions. IET Intelligent Transport Systems **15**, 1215–1227 (2021). DOI 10.1049/itr2.12085
6. Xue, Z., Li, C., Wang, X., Li, L., Zhong, Z.: Coordinated control of steer-by-wire and brake-by-wire for autonomous emergency braking on split-μ roads. IET Intelligent Transport Systems **14**, 2122–2132 (2020). DOI 10.1049/iet-its.2020.0184
7. Šabanovič, E., Žuraulis, V., Prentkovskis, O., Skrickij, V.: Identification of road-surface type using deep neural networks for friction coefficient estimation. Sensors **20**(3), 612 (2020)
8. Klomp, M.: On drive force distribution and road vehicle handling - a study of understeer and lateral grip. Licentiate thesis, Chalmers University of Technology (2007). URL https://research.chalmers.se/publication/62283
9. Rajamani, R.: Vehicle dynamics and control. Springer Science & Business Media (2011)